

Measuring the cosmological constant with redshift surveys

W. E. Ballinger¹, J. A. Peacock² and A. F. Heavens¹

¹ *Institute for Astronomy, University of Edinburgh, Blackford Hill, Edinburgh EH9 3HJ, UK*

² *Royal Observatory, Blackford Hill, Edinburgh EH9 3HJ, UK*

26 November 2024

ABSTRACT

It has been proposed that the cosmological constant Λ might be measured from geometric effects on large-scale structure. A positive vacuum density leads to correlation-function contours which are squashed in the radial direction when calculated assuming a matter-dominated model. We show that this effect will be somewhat harder to detect than previous calculations have suggested: the squashing factor is likely to be < 1.3 , given realistic constraints on the matter contribution to Ω . Moreover, the geometrical distortion risks being confused with the redshift-space distortions caused by the peculiar velocities associated with the growth of galaxy clustering. These depend on the density and bias parameters via the combination $\beta \equiv \Omega^{0.6}/b$, and we show that the main practical effect of a geometrical flattening factor F is to simulate gravitational instability with $\beta_{\text{eff}} \simeq 0.5(F - 1)$. Nevertheless, with datasets of sufficient size it is possible to distinguish the two effects. We discuss in detail how this should be done, and give a maximum-likelihood method for extracting Λ and β from anisotropic power-spectrum data. New-generation redshift surveys of galaxies and quasars are potentially capable of detecting a non-zero vacuum density, if it exists at a cosmologically interesting level.

Key words: Cosmology: theory – large-scale structure of Universe

1 INTRODUCTION

In recent years there has been a resurgence of interest in the cosmological constant Λ as a possible way of evading several cosmological problems (see Carroll et al. 1992 for a review). Although long popular with theorists, the Einstein-de Sitter $\Omega_m = 1$ model (hereafter denoted EdS) now seems increasingly untenable owing to its short expansion timescale. An open model with low matter density parameter Ω_m and no cosmological constant allows a younger universe, but is more difficult to reconcile with inflation. Although some workers have suggested that bubble nucleation within inflation may be capable of yielding an open universe (e.g. Bucher, Goldhaber & Turok 1995), a more common alternative to the EdS model is to retain a flat universe, $k = 0$, through $\Omega \equiv \Omega_m + \Omega_\Lambda = 1$. A high value of $\Omega_\Lambda \simeq 0.8$ would then be indicated by arguments for $\Omega_m \simeq 0.2$ from cluster M/L values and large-scale structure measurements (Efstathiou, Sutherland & Maddox 1990). In any case, it must be remembered that there is no known reason for the vacuum density to vanish (Weinberg 1989), and so it is profoundly important for physics to test whether Λ is non-zero.

It has been suggested by Alcock & Paczyński (1979) that it may be possible to detect the presence of Λ by a geometric test, measuring the effect of deviations from the assumed EdS geometry on large scale structure. The assump-

tion of an incorrect geometry can lead to an effective squashing of space along the line of sight – causing an anisotropy in the inferred density field which could be detected from galaxy (or quasar) clustering statistics. This has the crucial advantage over other tests such as number counts of being independent of galaxy or quasar evolution. Phillipps (1994) considered the possibility of analysing a quasar survey using the orientation of pairs and claimed that the effect should be readily detectable. However, the only cosmological constant model discussed by Phillipps is de Sitter space: zero mass density and $\Omega_\Lambda = 1$. We show that if the matter density parameter is even modestly greater than zero then the geometric effect is much reduced and also does not continue to increase with redshift above $z \simeq 1$.

Redshift-space distortions caused by peculiar velocities of galaxies also lead to anisotropic structure. Large-scale infall squashes overdensities along the line of sight in redshift space, which can mimic the geometric squashing caused by Λ . In the linear regime this distortion has a simple effect in Fourier space in the ‘distant observer’ approximation (see Kaiser 1987) and is characterised by the parameter $\beta = \Omega_m^{0.6}/b$ (where b is the bias parameter). For parameters of interest, redshift distortion is not negligible in comparison with the geometric distortion. The situation is complicated further on small scales, where virialized clusters appear elongated along the line of sight – the so-called ‘fingers of God’.

We therefore consider in some detail the clustering anisotropies which arise in the presence of all three effects: geometric flattening, β -distortion and fingers of God. We use a power spectrum analysis, since the modelling of redshift-space distortions is simpler in Fourier space than it is in real space. Although the Kaiser and squashing effects are similar, the functional forms of the anisotropies in the power spectrum differ, and Λ and β can be distinguished in principle. Sections 2 & 3 plus Appendix A give the basics of the effect. In Section 4, we present a maximum-likelihood technique for measuring both Λ and β from these anisotropies in Fourier space. Finally, in Section 5, we give some assessment of the likely practical constraints on Λ that may be expected from next-generation redshift surveys, such as the Anglo-Australian 2-degree field survey and the Sloan Digital Sky Survey.

2 COSMOLOGICAL MODELS AND CLUSTERING ANISOTROPY

To measure the cosmological constant, we exploit the fact that we cannot measure comoving distances directly, but use redshift as a distance indicator. An object which is spherical in comoving real space \mathbf{r} will only appear spherical to an observer (who measures redshifts) if the correct geometry is assumed – i.e. the correct $r(z)$ relation is used.

We write the Robertson-Walker metric as:

$$ds^2 = c^2 dt^2 - R(t)^2 [dr^2 + S_k^2(r) (d\theta^2 + \sin^2\theta d\phi^2)]. \quad (1)$$

Here $R_0 r$ is the comoving geodesic distance, $R(t)$ is the cosmic scale factor (= R_0 now) and :

$$S_k(r) = \begin{cases} \sin r & k = 1 \quad \text{closed} \\ r & k = 0 \quad \text{flat} \\ \sinh r & k = -1 \quad \text{open} \end{cases} \quad (2)$$

The square of the comoving distance between two objects at $z \pm \Delta z/2$ separated by $\Delta\theta$ is:

$$\Delta\ell^2 = R_0^2 S_k(r)^2 \Delta\theta^2 + R_0^2 \left(\frac{dr}{dz} \right)^2 \Delta z^2 \quad (3)$$

For a universe with matter contribution Ω_m and cosmological constant contribution Ω_Λ :

$$R_0 \frac{dr}{dz}(z) \equiv A_t(z) = \frac{c}{H_0} \frac{1}{\sqrt{(1-\Omega)(1+z)^2 + \Omega_\Lambda + \Omega_m(1+z)^3}} \quad (4)$$

$$R_0 S_k(r) \equiv B_t(z) = \frac{c}{H_0} |1-\Omega|^{-1/2} \times \left[S_k \left[\int_0^z \frac{|1-\Omega|^{1/2} dz'}{\sqrt{(1-\Omega)(1+z')^2 + \Omega_\Lambda + \Omega_m(1+z')^3}} \right] \right] \quad (5)$$

For flat models, favoured by inflation, $\Omega = \Omega_m + \Omega_\Lambda = 1$, so:

$$R_0 \frac{dr}{dz}(z) = \frac{c}{H_0} \frac{1}{\sqrt{(1-\Omega_m) + \Omega_m(1+z)^3}} \quad (6)$$

$$R_0 r(z) = \frac{c}{H_0} \int_0^z \frac{dz'}{\sqrt{(1-\Omega_m) + \Omega_m(1+z')^3}} \quad (7)$$

Even with this simplification, the integral for $R_0 r(z)$ must be carried out numerically unless $\Omega_\Lambda = 0$ or $\Omega_m = 0$.

There are three coordinate systems to consider here. We denote by the subscript t the true geometry, where z represents the redshift from pure Hubble expansion at the coordinate distance r . We denote by s the coordinate system where the geometry is correct, but the redshift is used as a distance indicator. This incorporates redshift distortion from peculiar velocities. Finally, we denote by the subscript a the assumed geometry. This will always be an EdS model in the present paper, and quoted flattening factors are given relative to this model, for which we have

$$R_0 \frac{dr}{dz}(z) = \frac{c}{H_0} \frac{1}{(1+z)^{3/2}} \equiv A_a(z) \quad (8)$$

$$R_0 r(z) = 2 \frac{c}{H_0} \left(1 - \frac{1}{\sqrt{1+z}} \right) \equiv B_a(z) \quad (9)$$

Taking EdS as default, we define geometric squashing factors:

$$f_{\parallel}(z) \equiv \frac{A_t}{A_a} \quad (10)$$

$$f_{\perp}(z) \equiv \frac{B_t}{B_a} \quad (11)$$

$$F(z) \equiv \frac{f_{\parallel}}{f_{\perp}} = 1 + \frac{1}{4}(1 - \Omega_m + 2\Omega_\Lambda)z + O(z^2) \quad (12)$$

f_{\perp} , f_{\parallel} and F are all unity for EdS. The flattening factor F is defined so that $F > 1$ means that objects would appear flattened along the line of sight in the assumed geometry. The first-order redshift dependence (obtained with the aid of *Mathematica*) tells us that what is really measured via the flattening is not Ω_Λ but $\Omega_\Lambda - \Omega_m/2$. This is inevitable, since a general argument (e.g. section 14.6 of Weinberg 1972) shows that the lowest-order corrections to the distance-redshift relation depend only on $q_0 = \Omega_m/2 - \Omega_\Lambda$. The accuracy with which one can measure Ω_Λ from low-redshift data is then limited by (amongst other things) one's knowledge of Ω_m , which is currently rather poorly known. In principle, measuring the evolution at several redshifts out to $z > 1$ would allow both Ω_m and Ω_Λ to be determined separately, but this will be harder. It is also interesting to compare the Ω_m dependence in the case of open and flat models: $F \simeq 1 + (1 - \Omega_m)z/4$ with $\Omega_\Lambda = 0$ but the three-times stronger $F \simeq 1 + 3(1 - \Omega_m)z/4$ for $k = 0$.

It can be seen from Fig. 1a and Fig. 1b that the squashing effect of Λ (characterised by F) increases rapidly with redshift and then saturates at redshift of $z \simeq 1$ for all but pure de Sitter space ($\Omega_m = 0$). The fact that F does not increase without limit if $\Omega_m \neq 0$ is easily understood. At high redshifts matter dominates over vacuum energy because of their equations of state, and

$$\frac{\Omega_m(z)}{\Omega_\Lambda(z)} \propto (1+z)^3. \quad (13)$$

Hence at high z , the cosmological constant becomes insignificant. The saturation is quite severe: $F \leq 1.3$ for $\Omega_m \geq 0.2$ (the limit of most current models). Compare this with the de Sitter model which reaches $F = 2.2$ at $z = 2$. There is therefore unlikely to be any gain by going to very high redshifts: a galaxy survey with a large number of galaxies may well be preferable to a deeper but much smaller quasar survey.

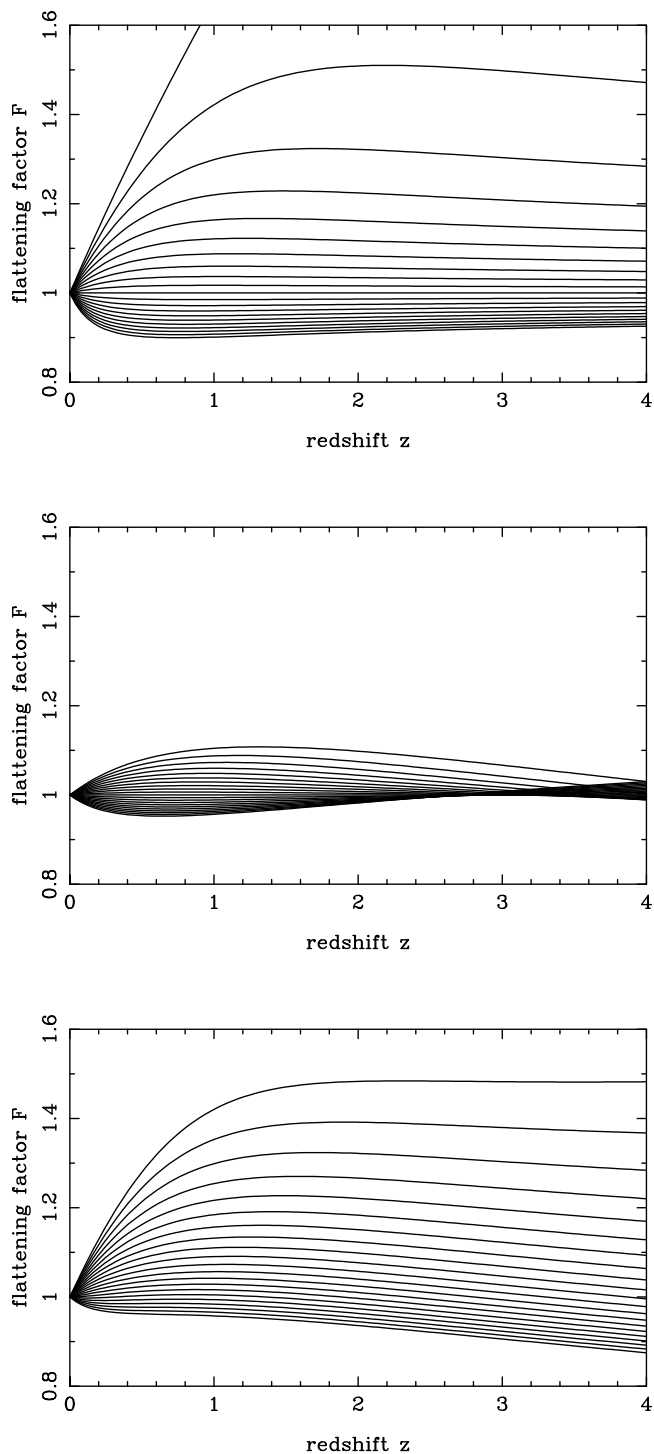


Figure 1. (a) Flattening factor F as a function of redshift for flat models ($\Omega_m + \Omega_\Lambda = 1$). The curves range from $\Omega_\Lambda = 1$ (top curve) to $\Omega_\Lambda = -1$ in steps of 0.1. (b) F against redshift for models with a fixed mass density $\Omega_m = 0.2$ and a cosmological constant. Ω_Λ varies as for (a). (c) F against redshift for models with no cosmological constant. Ω_m varies from 0 (top) to 2, again in steps of 0.1.

The calculations can be repeated for open models with no cosmological constant, but the effects are much smaller (see Fig. 1c). Hence a large value of F indicates a cosmological constant, and would be a valuable robust measure of Λ , if it were not subject to confusion with other effects.

To utilise the squashing as a diagnostic for the geometry, it is necessary to have something of known shape. A convenient such object is the power spectrum of galaxy (or quasar) clustering, whose contours in \mathbf{k} -space must be spherical if the cosmological principle holds (although a survey which covered a significant range of redshifts would require power to be measured separately in a number of redshift bins to avoid anisotropy introduced by evolution). Denoting the real comoving wavenumber by \mathbf{k} , and splitting it into a component k_\parallel along the line-of sight and a component k_\perp perpendicular to it, the true comoving real space power spectrum will be a function only of $|k|$:

$$P_t(k_\parallel, \mathbf{k}_\perp) = P_t(k). \quad (14)$$

If we assume the wrong geometry, we measure power at the wrong wavelengths. Ignoring redshift distortions for the time being:

$$P_a(k_\parallel, \mathbf{k}_\perp) = \frac{1}{f_\perp^{3+n} F} P_t(k) \left[1 + \mu_a^2 \left(\frac{1}{F^2} - 1 \right) \right]^{\frac{n}{2}}, \quad (15)$$

where n is the local spectral index of the power spectrum and $\mu_a = \cos$ of wavevector to line of sight. This expression is derived in Appendix A, but is immediately reasonable: $P(\mu_a = 0)/P(\mu_a = 1) = F^n$, as expected for squashing by a factor F . This equation implies that there is no sensitivity to geometry for an $n = 0$ spectrum; however, this ceases to be true in the presence of peculiar velocities, which also give rise to power-spectrum anisotropies.

3 REDSHIFT DISTORTIONS

3.1 Linear Modes

In models where structure forms via gravitational instability, density fluctuations inevitably induce peculiar velocities, which affect the mapping to redshift space where the radial coordinate is a total velocity. In linear theory, density waves are boosted along the line of sight in redshift space (Kaiser 1987). We assume that the survey subtends a small angle in the sky and lines of sight can be treated as parallel, so that the simple Kaiser formula remains valid (see Heavens & Taylor 1995 and Zaroubi & Hoffman 1996 for more general analyses) – i.e. even with the correct assumed geometry, there is still anisotropy in redshift space:

$$P_s(k, \mu) = P_t(k)[1 + \beta\mu^2]^2 \quad (16)$$

where P_t is the isotropic real-space power spectrum and P_s is the power spectrum in the correct geometry.

This boosts the power spectrum along the line of sight as does the Λ effect, but it is clear from formulae (15) and (16) that the μ -dependence is different. Gravitational instability generates a characteristic ratio between the μ^2 and μ^4 components, which differs in general from that resulting from geometrical distortion. Hence the two effects are distinguishable in principle, given data of sufficiently high signal-to-noise (see Fig. 2).

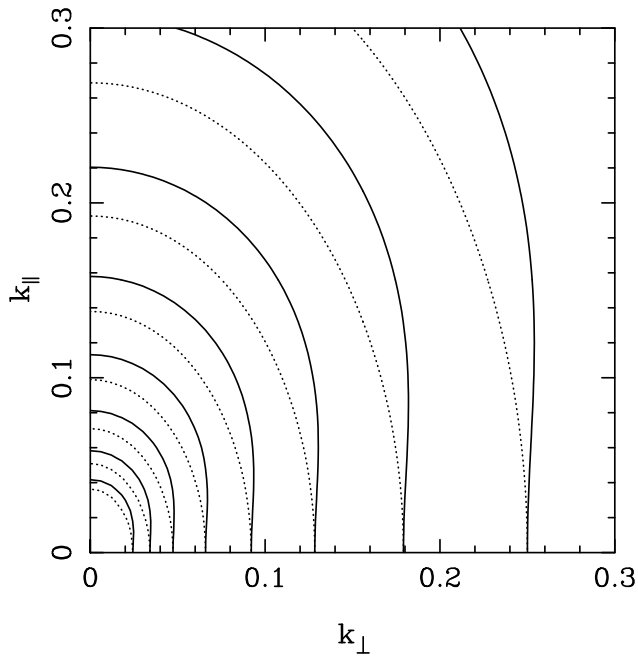


Figure 2. Contours of the power spectrum in the k_{\parallel} and k_{\perp} plane, assuming a power-law index $n = -1.5$ for the true power spectrum. The contour interval is $\Delta \ln P = 1/2$. The models are linear (Kaiser) redshift distortion only with $\beta = 0.5$ (full contours) and geometric squashing effect only, with $F = 1.5$ (dotted contours).

3.2 Fingers of God

Additionally, we consider the nonlinear finger-of-God effect caused by velocity dispersions in virialized clusters. A simple model for the effects of such velocities on the power spectrum was introduced by Peacock (1992; see also Peacock & Dodds 1994). This consists of multiplying the linear-theory Kaiser distortion by a term which treats the radial distortion as a convolution with an incoherent velocity component, leading to damping of power at large values of k_{\parallel} :

$$P_s(k, \mu) = P_t(k) [1 + \beta \mu^2]^2 D[k\mu\sigma_p]. \quad (17)$$

If the dispersion is taken to be Gaussian, the damping term is

$$D[k\mu\sigma_p] = \exp[-k^2 \mu^2 \sigma_p^2 / 2]. \quad (18)$$

Here σ_p is the line-of-sight *pairwise* dispersion in relative galaxy velocities caused by the incoherent dispersion ($\sigma_p = \sqrt{2}\sigma_v$). This is usually quoted in velocity units, but is implicitly divided by 100 to obtain a scale-length in $h^{-1}\text{Mpc}$ when used in power spectra*. Note that it is not obvious that this parameter corresponds exactly to the pairwise velocity dispersion measured using other methods, although it should be close. In reality, the pairwise velocity distribution is better modelled by an exponential (Davis & Peebles 1983), which leads to a Lorentzian factor in Fourier space:

* Hubble constant $H_0 = 100 h \text{ kms}^{-1} \text{Mpc}^{-1}$

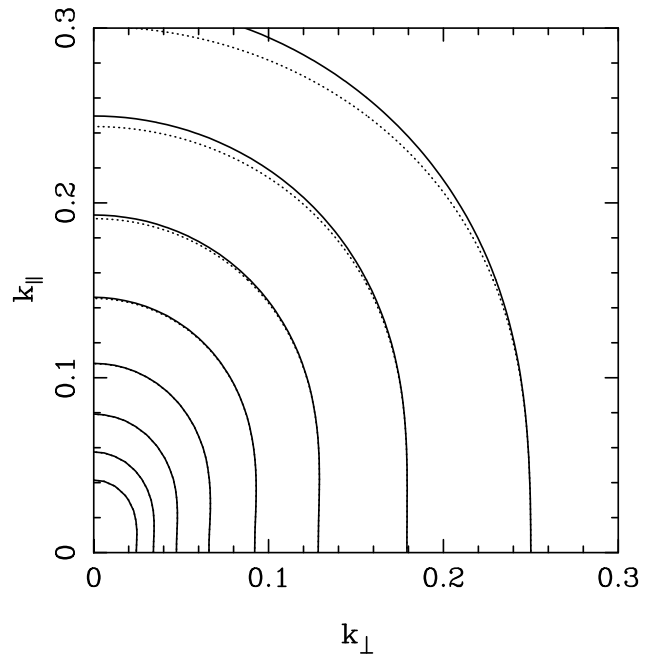


Figure 3. Contours for both linear and nonlinear redshift distortions with $\beta = 0.5$, and $\sigma_p = 350 \text{ kms}^{-1}$ (again for $n = -1.5$). The solid contours are for exponential small scale velocity distribution, the dotted Gaussian. The contour interval is $\Delta \ln P = 1/2$. The stretching of contours of the correlation function along the line of sight leads to a reduction in line of sight power on small scales (large k) – see also Cole, Fisher & Weinberg (1994).

$$D[k\mu\sigma_p] = \frac{1}{1 + (k\mu\sigma_p)^2 / 2}. \quad (19)$$

In practice, there is very little difference between these models until the damping becomes a factor $\gtrsim 2$ – see Fig. 3. According to a comparison with N -body simulations by Cole, Fisher & Weinberg (1994) and (1995) (hereafter CFW94 and CFW95), this simplified analytical model appears to work well up to $k\sigma_p$ of order unity. We note that CFW95 in fact use a damping factor of a Lorentzian squared, which is not equivalent to an exponential pairwise distribution (it actually corresponds to an exponential one-particle distribution); however, this makes very little difference to the answers.

3.3 The general case

Combining the effects of geometry, linear peculiar velocities and fingers of God, it is shown in Appendix A that the overall effect is

$$P_a(k, \mu) = \frac{1}{f_{\perp}^{3+n} F} P_t(k) \left[1 + \mu^2 \left(\frac{1}{F^2} - 1 \right) \right]^{\frac{n-4}{2}} \times \left[1 + \mu^2 \left(\frac{\beta+1}{F^2} - 1 \right) \right]^2 D[k\mu\sigma'_p], \quad (20)$$

where $\sigma'_p \equiv \sigma_p / f_{\parallel}$, and we have modified μ to account for the assumed geometry. If $\beta = 0$, and F is close to unity, then the anisotropy resembles a pure redshift-space distortion, with an apparent value of β :

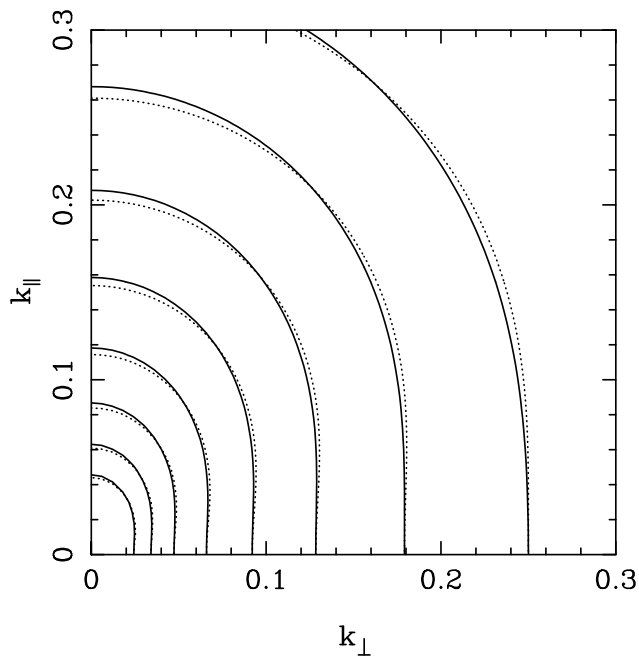


Figure 4. Solid contours for a model with $F = 1.1$, $\beta = 0.5$ and $\sigma_p = 350 \text{ km s}^{-1}$. Dotted contours are for the best fit to this model with redshift distortions only ($F = 1$).

$$\beta_a \simeq -\frac{n}{2}(F - 1). \quad (21)$$

If the true β is small but non-zero, then the true distortion adds linearly to the geometrical signature; for large β , things are more complex, since F also modifies the effect of β . Since the effective $n \simeq -1$ on the scales of interest where β can be measured, we see that any experiment which hopes to detect Λ through $F \simeq 1.3$ will need to be able to measure β_a to a precision of rather better than ± 0.1 . Fig. 4 shows that the differences between the F and β effects are subtle; a large survey with good statistical signal-to-noise will be needed if the two effects are to be measured separately. Furthermore, because the effects of interest are small, careful control of systematics will be required. For example, one will not wish to assume the precise correctness of the model (17) for the redshift-space distortions, and empirical relations from numerical simulations will be more appropriate. However, for the present the simple model suffices to indicate how hard we will have to work. It also illustrates how well one needs to know the intrinsic shape of the objects whose flattening is being exploited. The scatter in the shapes of cosmic objects such as voids (cf. Ryden 1995) will preclude their use for this purpose.

3.4 Geometry from evolution of β

Although we have shown that F and β are degenerate to some extent at a single redshift, they are expected to evolve differently. This in itself does not help to detect Λ , because the evolution of bias is unknown:

$$\beta(z) = \frac{\Omega_m^{0.6}(z)}{b(z)}. \quad (22)$$

Nusser & Davis (1994) have argued that $b(z)$ is calculable provided galaxy numbers are preserved; however, we feel it is better not to assume that merging is negligible and to treat the evolution of bias empirically. This argues that we must seek a signature of Λ which takes the empirical $\beta(z)$ without seeking to assume what fraction of the evolution is due to changes in Ω_m with redshift. The following sections of this paper are devoted to seeing what can be done by looking at the detailed μ -dependence of the clustering anisotropies, in order to break the lowest-order degeneracy.

However, further information on $b(z)$ can be obtained from the evolution of the amplitude of the power spectrum with redshift, as discussed by Matsubara & Suto (1996). In the linear regime, the true galaxy power spectrum evolves as

$$P_t(z) = b^2(z)P_{\text{mass}}(z) = \frac{b^2(z)}{b^2(0)}\mathcal{D}^2(z)P_t(0), \quad (23)$$

where $\mathcal{D}(z)$ is the linear-theory growth law for density perturbations. Unfortunately, this evolution is not directly measurable: even looking at real-space clustering, there are geometrical factors which alter the inferred clustering (cf. the $\mu = 0$ limit of equation [20]); what is observable is thus the apparent growth factor

$$\mathcal{D}_a(z) = \frac{b(z)}{b(0)} \frac{\mathcal{D}(z)}{[f_{\perp}^{3+n}(z)F(z)]^{1/2}}. \quad (24)$$

The other observable is the apparent redshift-space distortion as a function of redshift, which we choose to describe by an apparent value of β . If the true β is of order unity, then the geometrical and velocity distortions interfere in a complex manner. Suppose we deduce an apparent β by fitting $P(\mu)/P(\mu = 0)$ by a velocity-only distortion; to first order in $(F - 1)$, this gives an apparent value of β

$$\beta_a(\mu) = \beta - \left[2\beta(1 - \mu^2) + \frac{n}{2}(1 + \beta\mu^2) \right] (F - 1). \quad (25)$$

There are thus many possible choices of β_a ; the simplest procedure is probably to average these choices over μ , yielding the redshift-dependent observable

$$\beta_a(z) = \beta(z) - \frac{8\beta(z) + [3 + \beta(z)]n}{6}(F(z) - 1). \quad (26)$$

For a given hypothetical $(\Omega_m, \Omega_\Lambda)$ pair, the equations for $\beta_a(z)$ and $\mathcal{D}_a(z)$ both yield $b(z)/b(0)$; requiring these curves to match at all z can in principle allow both density parameters to be determined.

It is interesting to explore this possibility in a little more detail by looking at the first-order change with redshift of these relations. The initial change with redshift of the observables are respectively

$$\frac{d\mathcal{D}_a}{dz} = -\Omega_m^{0.6} - \frac{n+4}{8}[1 - \Omega_m + 2\Omega_\Lambda] + \frac{d \ln b}{dz} \quad (27)$$

and

$$\frac{d\beta_a}{dz} = \left[\frac{4\beta}{15} - \frac{n}{24}(3 + \beta) \right] (1 - \Omega_m + 2\Omega_\Lambda) - \beta \frac{d \ln b}{dz}. \quad (28)$$

The second of these depends just on q_0 , but the first involves a different combination of Ω_m and Ω_Λ . If we eliminate the unknown bias evolution $d \ln b / dz$ from the above equations, we get

$$\Omega_m^{0.6} = -\frac{d\mathcal{D}_a}{dz} - \frac{d \ln \beta_a}{dz} - \left[\frac{7}{30} + \frac{n}{6} + \frac{n}{8\beta_a} \right] (1 - 2q_0). \quad (29)$$

For plausibly realistic values $n \simeq -1$, $\beta \simeq 0.5$, the coefficient of $(1 - 2q_0)$ is very small, giving a diagnostic for Ω_m alone. Studies of clustering evolution and anisotropy out to $z \simeq 0.5$ may thus principally determine Ω_m , rather than Ω_Λ . In order to pin down the cosmological constant, it will be necessary either (a) to work at $z \gtrsim 1$; (b) to work at large scales where $n \simeq 0$; or (c) to look in more detail at the angular dependence of the anisotropies. We now return to the last of these options.

4 MAXIMUM LIKELIHOOD FITTING

Given the model (20) for the combined geometrical plus redshift-space distortions, the standard way of proceeding would be to perform a maximum-likelihood fit on a dataset to obtain the required parameters $\beta, F, \sigma'_p = \sigma_p/f_{\parallel}$ and a parameterized form for $P_t(k)$ simultaneously. Smaller uncertainties in the most interesting parameters such as β and F may be obtained if we use a priori knowledge of e.g. the shape of P_t , but in order to make a robust test for Λ , it is safer to obtain all the information we require from the same survey.

To apply maximum-likelihood methods, we need to know the probability distribution for the power. The central limit theorem implies that the observed power averaged over many independent modes will have a Gaussian distribution (even though single modes will be Rayleigh distributed for a Gaussian random field – see Feldman et al. 1994). Similarly, $\ln P$ would be expected to have a Gaussian distribution with variance $\sigma^2 = 1/N$ where N is the number of independent modes averaged over:

$$f(\ln P_a) d \ln P_a = \left(\frac{N}{2\pi}\right)^{\frac{1}{2}} \exp\left[-\frac{N}{2}(\ln P_a - \ln P'_a)^2\right] d \ln P_a, \quad (30)$$

where P_a is the observed power as a function of k and μ , $P'_a[k, \mu; \Lambda, \beta, \sigma'_p, P_t(k)]$ is the corresponding mean power of the model. In both cases, the powers are the *total* power, including shot noise. The likelihood estimator is then

$$\ln \mathcal{L}[\Lambda, \beta, \sigma'_p, P_t(k)] = \text{const.} - \frac{1}{2} \sum_{\text{modes}} (\ln P_a - \ln P'_a)^2; \quad (31)$$

in the continuum approximation, this becomes:

$$\ln \mathcal{L} = \text{const.} - \rho \int_0^{k_{\text{max}}} \pi k^2 dk \int_0^1 (\ln P - \ln P')^2 d\mu, \quad (32)$$

where ρ is the density of states in \mathbf{k} -space.

For a non-uniform selection function, the effective density of states is (Appendix B)

$$\rho_{\text{eff}} = \frac{[\int w \bar{n} d^3r]^2}{(2\pi)^3 \int w^2 \bar{n}^2 d^3r}. \quad (33)$$

where $\bar{n}(r)$ is the mean density of objects, and $w(r)$ is the optimal weighting function of Feldman et al. (1994) for measuring power: $w = (1 + \bar{n}P)^{-1}$. The integral is restricted to

a maximum value of $k = k_{\text{max}}$ to prevent excessive nonlinearity, in particular to avoid wavenumbers where the ansatz for the fingers of God may not be a good approximation. CFW95 showed that this limit corresponds to $k\sigma'_p \lesssim 1.6$ (10 per cent error in the derived β). The precise maximum wavenumber allowed by this criterion depends on the assumed σ_p . Taking a conservative view of this, we will generally set $k_{\text{max}} = 0.35 h \text{Mpc}^{-1}$ as a safe limit within which F is not significantly affected by systematics in the inferred β . The sum/integral is over a hemisphere in k -space. The modes in the other hemisphere are identical: $P(\mathbf{k}) = P(-\mathbf{k})$ because the density field is real.

The procedure in practice is to maximise \mathcal{L} to find the best fitting parameters Λ , β , σ'_p and $P_t(k)$. We assume a shape for $P_t(k)$ and fit only for the amplitude, although the shape could be parameterized for a more extensive analysis. In this paper we are interested principally in the errors on the parameters, to work out whether any given survey will be able to distinguish between cosmological models of interest.

4.1 Covariances and Correlation matrix

We now wish to study the form of the likelihood contours that describe the joint distribution of the interesting parameters in this problem. This question can be studied in the absence of data because of the simple form of the likelihood function, which is a sum of squared differences in $\ln P$, multiplied by the density of states in k space. For a given observed power, the likelihood thus scales simply with the volume of the survey; the likelihood contours are of a fixed form, which are merely re-labelled as the number of modes increases. The covariance matrix C_{ij} for the parameters a_i is thus of a universal shape which can be scaled once the absolute value of the error on one parameter is known (at least for a fixed ratio of true power to shot power).

Even the effect of shot noise is rather weak. It only enters at all because the error in power scales with the power: $\sigma(P)$ thus changes with μ in the presence of redshift-space anisotropies, provided shot noise is negligible. Conversely, if shot-noise dominates, $\sigma(P)$ is a constant. In one limit, therefore, the likelihood measures the sum of $[\Delta \ln P]^2$, whereas in the other it is $[\Delta P]^2$. In practice, the difference seems to be small, as shown in Figs 5 & 6. The optimally-weighted QDOT dataset has $P_{\text{shot}} = P_{\text{true}}$ at $k = 0.05 h \text{Mpc}^{-1}$ and $P_{\text{shot}} = 10P_{\text{true}}$ at $k = 0.2 h \text{Mpc}^{-1}$. Future large-scale surveys are likely to have negligible shot noise on all quasi-linear scales.

To produce likelihood contours requires some data for the ‘observed’ power. In what follows, we simply take this to be the expected power in the model under consideration. A more exact procedure would be to produce a realization of the model, with the power for each mode exponentially distributed about the expectation value. The maximum-likelihood value of the parameters a_i obtained by fitting to such a fictitious dataset would then differ from the input ones, within the ‘error bars’ produced by the likelihood analysis. However, these errors are the same whether we input the expectation spectrum as data, or use a realization:

$$\begin{aligned} \Delta \ln \mathcal{L} &= -\frac{1}{2} \sum (\ln P_{\text{obs}} - \ln P_{\text{mod}})^2 \\ \Rightarrow C_{ij}^{-1} &= - \left. \frac{\partial^2 \ln \mathcal{L}}{\partial a_i \partial a_j} \right|_{ML} \simeq \sum \frac{\partial \ln P_{\text{mod}}}{\partial a_i} \frac{\partial \ln P_{\text{mod}}}{\partial a_j}, \end{aligned} \quad (34)$$

independent of the data. Note that this expression is only approximately true, since it assumes that the term $\sum (\ln P_{\text{obs}} - \ln P_{\text{mod}}) \partial^2 P_{\text{mod}} / \partial a_i \partial a_j$ is negligible. The maximum likelihood solution ensures that a somewhat different weighting of the data is zero: $\sum (\ln P_{\text{obs}} - \ln P_{\text{mod}}) \partial P_{\text{mod}} / \partial a_i = 0$. In what follows in this section, we neglect the additional term; the numerical results presented do not make this approximation. Using the expectation power spectrum as data therefore gives approximately the right error contours on the parameters, but centred on the input data. The constraints that can be set from a given real dataset would then depend on the actual maximum-likelihood values, which we would expect to be displaced from the true value by about the ‘one-sigma’ error calculated here.

Because the model power spectrum studied here is of a rather simple form, the covariance matrix can be obtained analytically in many cases, at least with the aid of a symbolic manipulator such as *Mathematica*. The general expressions are sufficiently messy that they are not worth reproducing, but there are a few exact results that are simple enough to be useful. First recall that the power to be fitted is the sum of a true power P_T plus shot power P_S ; one might therefore approximate the covariance matrix as follows, simply interpolating between the scaling of the results for zero shot noise and for dominant shot noise:

$$C_{ij} = \frac{2}{N} \left(C_{ij}^A + \frac{P_S}{P_T} C_{ij}^B \right), \quad (35)$$

where N is the total number of modes being considered (over a complete sphere in k space). The covariance matrices for the shot-free and shot-dominated cases (C^A and C^B respectively) depend on the number of parameters being fitted for. Perhaps the most optimistic case would seem to be the two-parameter model where only β and F are allowed to vary, assuming that both the damping σ_p and the amplitude of the power spectrum are known. The latter assumption is probably unreasonable, since the main manifestation of a non-zero β or non-unity F is to change the mean level of power; the real signature we are interested in is the power anisotropy. Within the likelihood methodology, this demands that we allow the amplitude of the spectrum to float as a third parameter which is integrated over when we consider the distribution of the interesting parameters β and F .

For this model, the covariance matrices in the shot-free and shot-dominated limits can be obtained analytically in the limit of small β , where both have the same form:

$$C_{\beta\beta}^A = C_{\beta\beta}^B = \frac{11025 n^2}{256 (-4 + n)^2} \beta^{-2}. \quad (36)$$

As we saw earlier when considering the quadrupole term, in this limit

$$C_{FF} = \frac{4}{n^2} C_{\beta\beta}, \quad (37)$$

so that β can be obtained with greater accuracy than F if $n \simeq -1$. If only β and F had been allowed to vary, both results would have been a factor $16/25$ smaller – reflecting the spurious accuracy that arises if the effects on the normalization of the power spectrum are ignored. As β increases, $\beta^2 C$

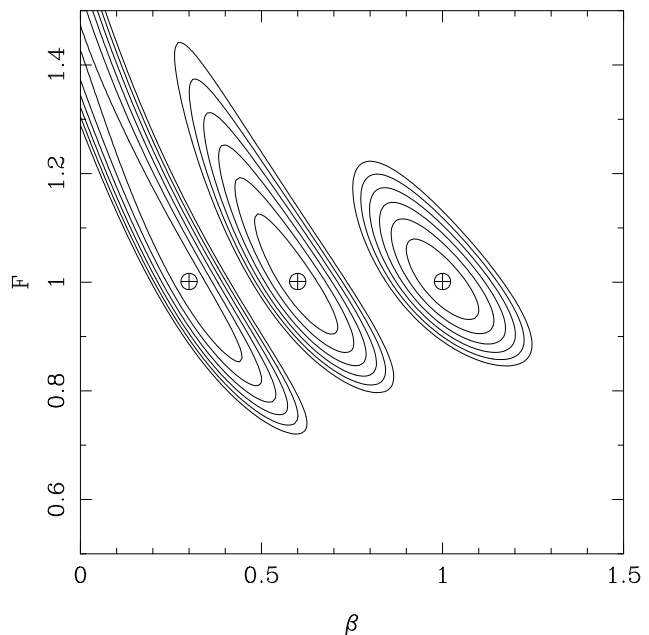


Figure 5. Expected contours of likelihood in the $F-\beta$ plane, for the case of a survey with negligible shot noise, for three values of β . The scaling is set so that $\sigma(\beta) = 0.1$ for $\beta = 1$. At each (β, F) point, the maximum-likelihood value of the power-spectrum amplitude has been chosen. The contour interval is $\Delta \ln \mathcal{L} = 1/2$. The position of the true values of the parameters is marked by the cross; contours are shown for $\beta = 0.3, 0.6$ and 1.0 .

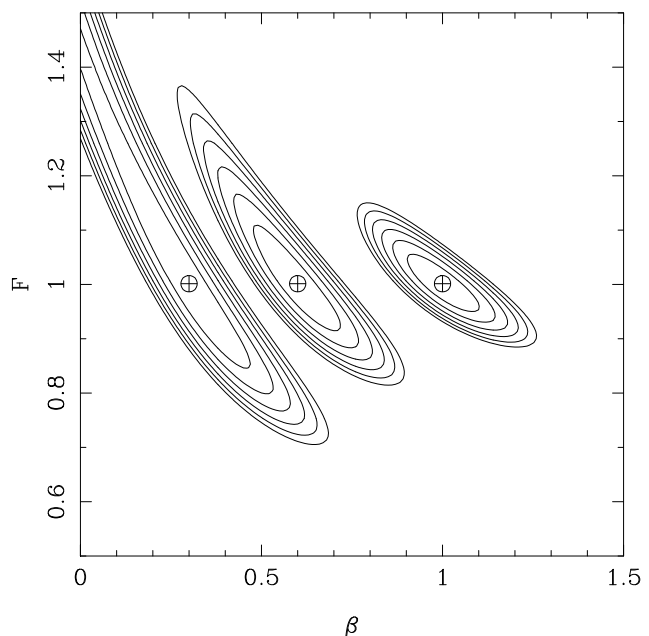


Figure 6. Expected contours of likelihood in the $F-\beta$ plane, as for Fig. 5 except now for the case of a survey dominated by shot noise.

changes approximately linearly with β , and it will suffice to quote the results at $\beta = 1$. For the shot-free case:

$$C_{\beta\beta}^A(\beta = 1) \simeq 22.4 - 16(n + 1.5), \quad (38)$$

$$C_{FF}^A(\beta = 1) \simeq 12.2 + 5(n + 1.5). \quad (39)$$

For the shot-dominated case, the numbers are smaller:

$$C_{\beta\beta}^B(\beta = 1) \simeq 10.8 - 6(n + 1.5), \quad (40)$$

$$C_{FF}^B(\beta = 1) \simeq 2.7 + (n + 1.5). \quad (41)$$

We see that, although $C_{\beta\beta}$ is smaller than C_{FF} when β is small, $\beta^2 C_{\beta\beta}$ increases quite significantly with β , whereas $\beta^2 C_{FF}$ increases slowly or even declines. If β is large, it is therefore possible to measure F more precisely than β .

The correlations between the parameters are described by the correlation matrix

$$r_{ij} = C_{ij} / \sqrt{C_{ii}C_{jj}}, \quad (42)$$

where $C_{ij} = \langle \delta a_i \delta a_j \rangle$, and no summation is implied in C_{ii} . At $\beta = 0$, β and F are perfectly anticorrelated, with $r_{\beta F}$ increasing as β increases. In the shot-free case, $r_{\beta F}(\beta = 1) \simeq -0.75 + 0.4[1.5 + n]$, whereas $r_{\beta F}(\beta = 1) \simeq -0.85 + 0.2[1.5 + n]$ when shot-noise dominates. This increase of the anti-correlation between F with β for lower values of β can be understood as follows: if we expand equation (20) in powers of μ , for small β and $\epsilon \equiv F - 1$, the coefficient of μ^2 is linear in β and ϵ , but gives degenerate information on these parameters. To separate β and ϵ requires at least the μ^4 term, which is of second-order smallness in β and ϵ .

These results all apply to long wavelengths, where the effects of the damping term are negligible. We give in Appendix C a selection of correlation matrices for this case, and also for the case where modes up to $k\sigma_p = 1$ are used, and σ_p is allowed to float as a further parameter. This makes rather little difference to the precision with which F can be determined (assuming the correctness of the model, of course). The long-wavelength results are illustrated in Figs 5 & 6, which show likelihood contours in the (β, F) plane where, at each (β, F) point, the amplitude distribution has been integrated over, but the value of σ_p is fixed. These are thus not just slices through the likelihood contours, but show the practical joint confidence region on F & β .

4.2 Evolutionary effects

In practice, measurable deviations from $F = 1$ will involve working over a significant range of redshifts where one may need to consider evolution of F , β etc. A practical means of dealing with this difficulty will be to divide the survey up into cubes, and use the zero-redshift value of Ω_Λ as a parameter. In each redshift shell, one should form the marginal distribution for Ω_Λ , integrating over other parameters as necessary, before combining all shells to estimate Ω_Λ – in a way that is by construction independent of evolution (an alternative would be to fit a functional form $\beta[z]$). It is the independence of the estimate of Λ on evolution which makes this method so attractive, as most other geometric tests of Λ require assumptions about evolution. In order to apply the Kaiser approximation, we require subsamples which subtend small angles on the sky; cubic subsamples will therefore also

have a small $\Delta z / (1 + z)$ and so it will be satisfactory to ignore evolution within each cube. The number of modes out to wavenumber k_{\max} scales as the box volume, so the number of modes studied is the same whether one large volume is studied, or many small sub-volumes. All that is lost is the signal from the very large-scale modes, but these are a negligible fraction of the total.

5 APPLICATIONS

5.1 Galaxies

The next few years should see a number of substantial new galaxy redshift surveys with which this test could be attempted. The IRAS PSCz survey of 15,000 galaxies (Saunders et al. 1995) will cover essentially 4π sr and will define the density field out to approximately $z \simeq 0.1$. This will not be likely to be so useful for our present purpose owing both to the high level of shot noise over such volumes and also to the low depth, so that $F \lesssim 1.05$ is expected. More promising is the Sloan survey of $\sim 10^6$ galaxies over π sr, which should provide a map free of shot noise out to $z \simeq 0.2$, or an effective volume of about $500^3 (h^{-1}\text{Mpc})^3$ (Gunn & Weinberg 1995). The AAT 2df facility (Taylor 1995) should provide a survey of slightly greater depth and approximately 1/6 the area, giving errors approximately twice as large as for the Sloan survey.

We have calculated likelihood contours for Ω_Λ for a model survey similar to the 2df survey assuming the same parameter values as in section 4.2, which is shown in Fig. 7. The survey is divided into cubes each subtending 13° – side $100 h^{-1}$ Mpc at $z = 0.2$ – the number of galaxies in each cube being derived from the APM selection function of Baugh & Efstathiou (1993) down to a magnitude limit of $B_J \leq 19.5$ (a surface density of approximately 150 per square degree). We have assumed for simplicity that β and σ_p do not vary with redshift; as discussed in section 4.2, this does not affect the precision in Ω_Λ that can be obtained.

We see that the 2df survey is potentially capable of ruling out the high values of $\Omega_\Lambda \simeq 0.8$ that are interesting for inflationary models. Much will depend on the true value of β (which will also be obtained, with exquisite precision). If $\beta \simeq 1$, the rms error on Ω_Λ is about 0.35, but this approximately doubles if $\beta \simeq 0.3$. In this latter case, even the full Sloan survey would barely suffice to detect the flattening effect. This is an ironic outcome, since confusion with the β effect is one of the principal difficulties in measuring the geometrical flattening. Nevertheless, the best hope for a positive geometrical detection comes precisely when the redshift-space distortions are highest.

5.2 Quasars

Again, both the Sloan and 2df projects are expected to provide large quasar samples: about 10^5 and 30,000 respectively. The larger redshifts probed mean that the anisotropy signal is expected to be significantly larger, and the volumes probed are larger, giving many more modes. However, the quasar samples will be strongly shot-noise limited, reflecting the low space densities of these tracers. In Fig. 8 we show results for 30,000 quasars over an area of 750 deg^2 , with

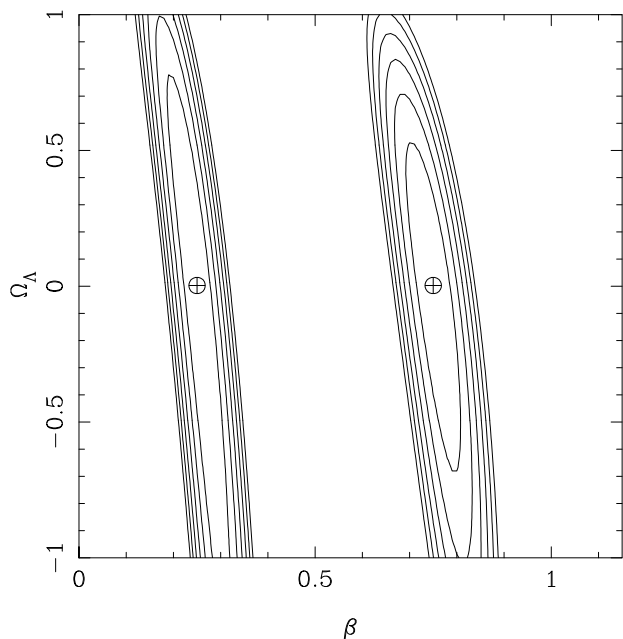


Figure 7. Expected contours of likelihood in the $\Omega_\Lambda - \beta$ plane for a 2df-type galaxy redshift survey of 250,000 galaxies to $B_J < 19.5$, obtained by combining cubic subsamples over a range of redshifts. Spatial flatness ($\Omega_m + \Omega_\Lambda = 1$) is assumed. The models shown assume true values for β of 0.25 and 0.75, and $\Omega_\Lambda = 0$, as indicated by the crosses.

a constant dN/dz over the redshift range $0.3 \leq z \leq 2.2$. For a given value of β , quasars put tighter constraints on a positive Ω_Λ than galaxies. The larger volume, and in particular the higher redshift, more than offset the increased shot noise, especially given that quasars are observed to be highly clustered at high redshift: – the clustering scale-length is claimed to be $r_0 \simeq 6 h^{-1}\text{Mpc}$ for quasars with $z < 2.2$ (Shanks & Boyle 1994).

For a particular β , the proposed quasar surveys thus have a strong advantage over the galaxy survey. However, β for quasars may well be smaller. The observed quasar clustering corresponds to $\sigma_8 \simeq 1.2$ at a mean redshift of $z \simeq 1.5$, whereas it is believed that the present value of σ_8 for mass is about $0.6\Omega_m^{-0.5}$; at redshift 1.5 this would be smaller by 2.5 times the Ω -dependent growth suppression factor (the exact form of which depends on both Ω_m and Ω_Λ). This increases the Ω_m dependence giving roughly:

$$\sigma_8(z = 1.5) \simeq 0.24 \Omega_m^{-0.8}, \quad (43)$$

approximately independent of Λ . If the ratio of the two σ_8 values is taken to measure the bias factor, then quasars are strongly biased at high z and the corresponding β is very low unless Ω_m is extremely low:

$$\beta_Q(z = 1.5) \simeq 0.2 \Omega_m^{-0.2} \quad (44)$$

However, inspection of Fig. 8a shows that, even if β for the quasars is low, they appear to be a better prospect for ruling out high- Ω_Λ models than the low-redshift galaxies. These calculations show that the advantage of having a larger signal at high redshift outweighs the twin disadvantages of higher shot noise and the (anticipated) lower value of β .

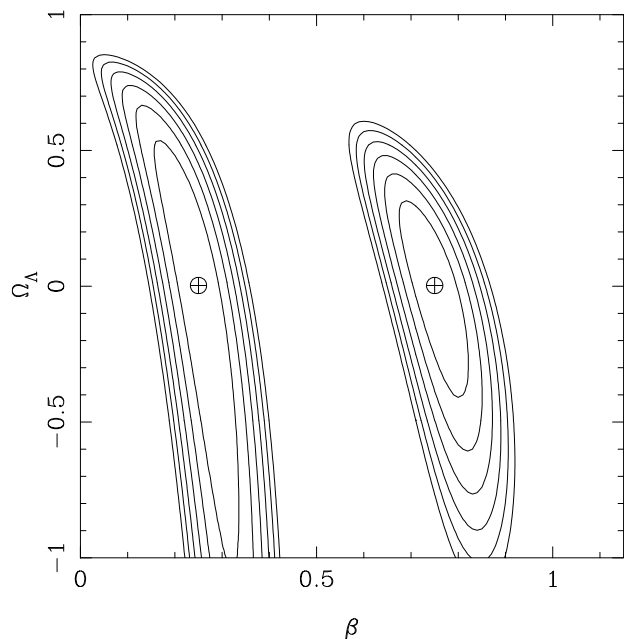


Figure 8. Expected contours of likelihood in the $\Omega_\Lambda - \beta$ plane for a 2df-type quasar survey of 30,000 quasars with $z < 2.2$. Spatial flatness ($\Omega_m + \Omega_\Lambda = 1$) is assumed. The models shown assume true values for β of 0.25 and 0.75, and $\Omega_\Lambda = 0$, as indicated by the crosses.

However, since the datasets are independent, the strongest result would come from combining the likelihoods for the two surveys.

We have assumed that $\sigma'_p = 350 \text{ km s}^{-1}$, as for the galaxy survey. If σ'_p were as low as 200 km s^{-1} (and this number should certainly decline with redshift, since it scales roughly linearly with σ_8) then $k_{\text{max}} = 0.8 h \text{ Mpc}^{-1}$ can be used ($k_{\text{max}}\sigma'_p = 1.6$). However, the constraints on Ω_Λ are little different from those of Fig. 8 – the power spectrum amplitude falls off towards small scales, hence the additional modes are swamped by the shot noise.

6 SUMMARY AND CONCLUSIONS

We have investigated in some detail the practical applicability of the original suggestion by Alcock & Paczyński (1979) that the cosmological constant might be measured via geometrical distortion of clustering at high redshift. We find that application of this method will be considerably more difficult than previous studies have suggested, for two reasons.

(1) The expectation that $\Omega_m \gtrsim 0.2$ limits the likely degree of anisotropy to a factor < 1.3 , at least for the spatially flat models popular from inflation.

(2) Without datasets of very large size and quality, it is difficult to distinguish the geometrical distortion from the redshift-space anisotropies induced by peculiar velocities.

In order to have a chance of distinguishing the two distortions, we have shown that it will be necessary to probe down to scales where the linear analysis of velocity-induced anisotropies is inadequate. We have used an approximate

model for such effects to show that datasets likely to become available in the next 5 years stand a good chance of being able to detect Λ . The exact probability of success depends critically on the degree of redshift-space distortion, with stronger signals expected if β is high. For $\beta = 1$, the AAT-2df galaxy redshift survey should be able to detect $\Omega_\Lambda \simeq 0.8$, whereas the full Sloan survey would only just suffice if $\beta \simeq 0.2$. Quasar surveys stand a better chance of success, provided β_Q is not $\ll \beta_G$. We may expect that surveys being completed now will shortly settle the controversy over at least β_G , giving a clearer idea of how well a geometrical search for Λ will work.

Although we have taken a pessimistic tone, showing that a test for Λ which is purely geometrical will be challenging, there are more optimistic aspects to our conclusions. The forthcoming surveys will give extremely precise measurements of $\beta(z)$, and this will certainly be a useful constraint: a given assumed Λ will then yield $b(z)$, and consistency with the evolution of the clustering amplitude with redshift should allow us to rule out some of these possible bias histories. However, the whole idea of Alcock & Paczyński's original suggestion was to avoid dealing with messy astrophysics, and we have shown that such a 'pure' test is still possible. This test will require a careful understanding of systematics in the redshift surveys, but we believe that it can be made into a reliable method for detecting large vacuum densities. At present, there is no competing method for estimating Λ in a way free from evolutionary uncertainties, so this route will continue to merit detailed scrutiny.

Acknowledgements

WEB acknowledges the support of a PPARC research studentship. Computations were done using STARLINK facilities.

REFERENCES

- Alcock C., Paczyński B., 1979 *Nature*, 281, 358
 Baugh C.M., Efstathiou G., 1993, *MNRAS*, 265, 145
 Bucher M., Goldhaber A.S., Turok N., 1995, *Phys. Rev. D*, 52, 3314
 Carroll S.M., Press W.H., Turner L.E., 1992, *ARA&A*, 30, 499
 Cole S., Fisher K.B., Weinberg D.H., 1994, *MNRAS*, 267, 785
 Cole S., Fisher K.B., Weinberg D.H., 1995, *MNRAS*, 275, 515
 Davis M., Peebles P.J.E., 1983, *ApJ*, 267, 465
 Efstathiou G., Sutherland W., Maddox S.J., 1990, *Nature*, 384, 705
 Feldman H.A., Kaiser N., Peacock J.A., 1994, *ApJ*, 426, 23
 Gunn J., Weinberg, D., 1995, in *Wide-field spectroscopy and the distant universe*, proc. 35th Herstmonceux conference, eds S.J. Maddox & A. Aragón-Salamanca, World Scientific, p3.
 Heavens A.F., Taylor A.N., 1995, *MNRAS*, 483, 497
 Kaiser N., 1987, *MNRAS*, 227, 1
 Lahav O., Lilje P.B., Primack J.R., Rees M.J., 1991, *MNRAS*, 251, 128
 Matsubara T., Suto Y., 1996, *ApJ*, in press
 Nusser A., Davis M., 1994, *MNRAS*, 421, L1
 Peacock J.A., Nicholson D., 1991, *MNRAS*, 253, 307
 Peacock J.A., Dodds S.J., 1994, *MNRAS*, 267, 1020
 Peacock J.A., 1992, in Martinez V., Portilla M., Sáez D., eds, *New insights into the Universe*, Proc. Valencia summer school (Springer, Berlin), p1
 Peebles P.J.E., 1980, *The Large Scale Structure of the Universe*. Princeton University Press, Princeton
 Phillipps S., 1994, *MNRAS* 269, 1077
 Ryden B., 1995, *ApJ*, 452, 25
 Saunders W., et al., 1995, in *Wide-field spectroscopy and the distant universe*, proc. 35th Herstmonceux conference, eds S.J. Maddox & A. Aragón-Salamanca, World Scientific, p88.
 Shanks T., Boyle B.J., 1994, *MNRAS*, 271, 753
 Taylor, K., 1995, in *Wide-field spectroscopy and the distant universe*, proc. 35th Herstmonceux conference, eds S.J. Maddox & A. Aragón-Salamanca, World Scientific, p15.
 Weinberg S., 1972, *Gravitation & Cosmology*, (New York: Wiley)
 Weinberg S., 1989, *Rev. Mod. Phys.*, 61, 1
 Zaroubi S., Hoffman Y., 1996, *Apj*, 462, 25

APPENDIX A: FOURIER TRANSFORMS

The squashing effect transforms coordinates and wave vectors as follows:

$$\mathbf{x}' = S \cdot \mathbf{x} \quad ; \quad \mathbf{k}' = S^{-1} \cdot \mathbf{k}, \quad (\text{A1})$$

with transformation matrix

$$S = \begin{pmatrix} f_{\perp}^{-1} & 0 & 0 \\ 0 & f_{\perp}^{-1} & 0 \\ 0 & 0 & f_{\parallel}^{-1} \end{pmatrix}. \quad (\text{A2})$$

The Λ squashing effect on the power spectrum is thus the following transform of the (possibly anisotropic) correlation function;

$$P(\mathbf{k}) = \int \xi(\mathbf{r}) e^{i\mathbf{k}\cdot\mathbf{r}} d^3r \quad (\text{A3})$$

$$P'(\mathbf{k}') = \int \xi(\mathbf{r}) e^{i(S\cdot\mathbf{k}')\cdot\mathbf{r}} |S| d^3r = |S| P(S \cdot \mathbf{k}'). \quad (\text{A4})$$

Note that $\xi'(\mathbf{r}') = \xi(\mathbf{r})$ since $\delta'(\mathbf{r}') = \delta(\mathbf{r})$. Apart from an amplitude shift the original power spectrum is retained, but evaluated at $S \cdot \mathbf{k}'$:

$$P'(k'_{\parallel}, \mathbf{k}'_{\perp}) = \frac{1}{f_{\perp}^2 f_{\parallel}} P\left(\frac{k'_{\parallel}}{f_{\parallel}}, \frac{\mathbf{k}'_{\perp}}{f_{\perp}}\right). \quad (\text{A5})$$

Redshift distortions are modelled as a product of a Kaiser factor and a damping term

$$\begin{aligned} P(k_{\parallel}, \mathbf{k}_{\perp}) &= P_0(k) (1 + \beta\mu^2)^2 D(k\mu\sigma_p) \\ &= P_0(k) k^{-4} [k_{\perp}^2 + (\beta + 1)k_{\parallel}^2] D(k_{\parallel}\sigma_p), \end{aligned} \quad (\text{A6})$$

where $D(k\mu\sigma_p)$ is the nonlinear ‘finger of God’ correction. Combining redshift and Λ effects gives

$$P'(\mathbf{k}') = \frac{1}{f_{\perp}^2 f_{\parallel}} P_0 \left(\sqrt{\frac{k_{\perp}'^2}{f_{\perp}^2} + \frac{k_{\parallel}'^2}{f_{\parallel}^2}} \right) \left(\frac{k_{\perp}'^2}{f_{\perp}^2} + \frac{k_{\parallel}'^2}{f_{\parallel}^2} \right)^{-2} \\ \times \left[\frac{k_{\perp}'^2}{f_{\perp}^2} + (\beta + 1) \frac{k_{\parallel}'^2}{f_{\parallel}^2} \right] D \left(\frac{k_{\parallel}' \sigma_p}{f_{\parallel}} \right). \quad (\text{A7})$$

Now we set $F = f_{\parallel}/f_{\perp}$, $k'_{\parallel} = \mu' k'$ and $\sigma'_p = \sigma_p/f_{\parallel}$, which yields

$$P'(\mathbf{k}') = \frac{1}{f_{\perp}^2 f_{\parallel}} P_0 \left[\frac{k'}{f_{\perp}} \sqrt{1 + \mu'^2 \left(\frac{1}{F^2} - 1 \right)} \right] \\ \times \left[1 + \mu'^2 \left(\frac{1}{F^2} - 1 \right) \right]^{-2} \\ \times \left[1 + \mu'^2 \left(\frac{\beta + 1}{F^2} - 1 \right) \right]^2 D(k' \mu' \sigma'_p). \quad (\text{A8})$$

For a power spectrum which is locally close to a power law, with index $n = d \ln P / d \ln k$, we have

$$P'(\mathbf{k}') = \frac{1}{f_{\perp}^{3+n} F} P(k') \left[1 + \mu'^2 \left(\frac{1}{F^2} - 1 \right) \right]^{\frac{n-4}{2}} \\ \times \left[1 + \mu'^2 \left(\frac{\beta + 1}{F^2} - 1 \right) \right]^2 D(k' \mu' \sigma'_p) \quad (\text{A9})$$

Assuming an exponential distribution for the random pairwise velocity component, the nonlinear correction to the power spectrum is a Lorentzian factor:

$$D(k' \mu' \sigma'_p) = \frac{1}{1 + (k' \mu' \sigma'_p)^2 / 2} \quad (\text{A10})$$

(where the units of σ'_p are $h^{-1} \text{Mpc}$).

APPENDIX B: SELECTION FUNCTIONS AND WEIGHTING SCHEMES

The number of independent modes depends on the details of the survey. We derive here the effective density of states for a varying selection function and weighting of the data. The simplest case is a uniformly sampled cube of side L , containing N_g galaxies, where independent modes are separated by $\Delta k = 2\pi/L$ in k space, so that:

$$\rho(k) = \left(\frac{L}{2\pi} \right)^3. \quad (\text{B1})$$

In this case (e.g. Peacock & Nicholson 1991), one would define Fourier coefficients via

$$\delta_{\mathbf{k}} = \frac{1}{N_g} \sum \exp[i\mathbf{k} \cdot \mathbf{x}], \quad (\text{B2})$$

and in the continuum limit we would have

$$\langle L^3 |\delta_{\mathbf{k}}|^2 \rangle = P_{\text{true}} + P_{\text{shot}} \quad (\text{B3})$$

where the shot noise depends on the density $n = N_g/L^3$:

$$P_{\text{shot}} = \frac{1}{n}. \quad (\text{B4})$$

In these expressions, we use the Fourier convention of Peebles (1980), but with unit normalization volume:

$$P(k) = \int \xi(r) \exp[i\mathbf{k} \cdot \mathbf{r}] d^3r. \quad (\text{B5})$$

These relations show that there is some advantage to having a large survey, thus giving a higher density of states. However, for a fixed number of galaxies, increasing the volume increases the shot noise on each mode. There is an optimum survey size for a given number of galaxies which corresponds to a signal-to-noise ratio of about unity.

The general case of a survey of non-uniform sampling was considered by Feldman et al. (1994; hereafter FKP). They also allow the galaxy density field to be weighted so as to optimise the signal-to-noise in the power spectrum:

$$\delta_{\mathbf{k}} = \frac{\int w[n - \bar{n}] \exp[i\mathbf{k} \cdot \mathbf{r}] d^3r}{\left[\int w^2 \bar{n}^2 d^3r \right]^{1/2}}, \quad (\text{B6})$$

where $\bar{n}(\mathbf{r})$ is the mean density defined by the sample selection. With this generalization,

$$\langle |\delta_{\mathbf{k}}|^2 \rangle = P_{\text{true}} + P_{\text{shot}} \quad (\text{B7})$$

where the shot noise is now

$$P_{\text{shot}} = \frac{\int w^2 \bar{n} d^3r}{\int w^2 \bar{n}^2 d^3r} \quad (\text{B8})$$

FKP also derive (their equation 2.3.2) the ratio of the variance in the total power to P_{true}^2 . For a uniform cubical survey of side L , this would be

$$\frac{\sigma(P)}{P_{\text{tot}}} = N_{\text{modes}}^{-1/2} = [\rho_k V_k]^{-1/2}, \quad (\text{B9})$$

which is proportional to $L^{-3/2}$. Converting the FKP result to the ratio of total variance to total power gives an effective survey size of

$$L_{\text{eff}}^{-3} = \frac{\int w^4 \bar{n}^4 [P + \bar{n}^{-1}]^2 d^3r}{\left[P \int w^2 \bar{n}^2 d^3r + \int w^2 \bar{n} d^3r \right]^2}. \quad (\text{B10})$$

This reduces to $L_{\text{eff}} = L$ for the previous case of a uniform cube. In general, we should use the optimal FKP weight $w = [1 + \bar{n}P]^{-1}$, which gives

$$L_{\text{eff}}^{-3} = \frac{\int w^2 \bar{n}^2 d^3r}{[\int w \bar{n} d^3r]^2}. \quad (\text{B11})$$

APPENDIX C: COVARIANCE MATRICES

We present here some example covariance matrices for the parameters p_i in the form of parameter standard deviations:

$$\sigma(p_i) = \sqrt{C_{ii}} \quad (\text{C1})$$

(no summation implied) and correlation matrices:

$$r_{ij} = C_{ij}/\sigma(p_i)\sigma(p_j) \quad (\text{C2})$$

for different combinations of values of β , slope n , and shot power to true power ratio at $k_{\text{max}} R = P_S/P_T$. The standard deviations are scaled such that $\sigma(\beta) = 1$ and the number of modes N required to achieve this accuracy is given. For a fixed R the standard deviations scale as $N^{-1/2}$. For example, if the volume of the survey is increased by a factor of 100, and k_{max} and the number density of galaxies were kept constant, the errors on the parameters would decrease by a factor of 10. We show covariances for both the three-parameter model with σ'_p fixed and the full four-parameter model where it is allowed to vary. The number of modes is kept constant when the number of parameters is changed, so the value of $\sigma(\beta)$ reflects the additional uncertainty introduced. All models have $k_{\text{max}}\sigma'_p = 1$ and $F = 1$.

C1 Example 1: $\beta = 1$; $n = -1.5$; $R = 0$; $N = 1120$

Table C1. Three-parameter model.

	β	F	$\ln A$
$\sigma(p)$	1.00	0.74	0.43
β	1.00	-0.76	-0.86
F	-0.76	1.00	0.56
$\ln A$	-0.86	0.56	1.00

Table C2. Four-parameter model.

	β	F	σ'_p	$\ln A$
$\sigma(p)$	1.38	0.75	2.52	0.42
β	1.00	-0.43	0.69	-0.63
F	-0.43	1.00	0.16	0.55
σ'_p	0.69	0.16	1.00	-0.01
$\ln A$	-0.63	0.55	-0.01	1.00

C2 Example 2: $\beta = 0.3$; $n = -1.5$; $R = 0$; $N = 3210$

Table C3. Three-parameter model.

	β	F	$\ln A$
$\sigma(p)$	1.00	1.14	0.24
β	1.00	-0.96	-0.73
F	-0.73	1.00	0.58
$\ln A$	-0.73	0.58	1.00

Table C4. Four-parameter model.

	β	F	σ'_p	$\ln A$
$\sigma(p)$	1.09	1.14	1.49	0.24
β	1.00	-0.87	0.41	-0.66
F	-0.87	1.00	-0.01	0.59
σ'_p	0.41	-0.01	1.00	0.00
$\ln A$	-0.66	0.59	0.00	1.00

C3 Example 3: $\beta = 1$; $n = -1$; $R = 0$; $N = 715$

Table C5. Three-parameter model.

	β	F	$\ln A$
$\sigma(p)$	1.00	1.01	0.53
β	1.00	-0.57	-0.86
F	-0.57	1.00	0.56
$\ln A$	-0.86	0.56	1.00

Table C6. Four-parameter model.

	β	F	σ'_p	$\ln A$
$\sigma(p)$	1.59	1.03	3.13	0.53
β	1.00	-0.23	0.78	-0.55
F	-0.23	1.00	0.16	0.55
σ'_p	0.78	0.16	1.00	-0.01
$\ln A$	-0.55	0.55	-0.01	1.00

C4 Example 4: $\beta = 1$; $n = -1.5$; $R = 1000$;
 $N = 855000$

Note that in this shot-noise dominated regime, the standard deviations scale with R to a good approximation for fixed N .

Table C7. Three-parameter model.

	β	F	$\ln A$
$\sigma(p)$	1.00	0.51	0.52
β	1.00	-0.85	-0.92
F	-0.85	1.00	0.65
$\ln A$	-0.92	0.65	1.00

Table C8. Four-parameter model.

	β	F	σ'_p	$\ln A$
$\sigma(p)$	1.02	0.51	1.35	0.52
β	1.00	-0.82	0.17	-0.91
F	-0.82	1.00	0.03	0.65
σ'_p	0.17	0.03	1.00	0.00
$\ln A$	-0.91	0.65	0.00	1.00